Hindawi
Laser and Particle Beams
Volume 2022, Article ID 4132792, 7 pages
https://doi.org/10.1155/2022/4132792

Research Article

Compact Thomson Scattering Source Based on a Mixed Injection Assisted Laser Wakefield Accelerator

Fang Tan, Xiao Hui Zhang, Bin Zhu, Gang Li, Yu Chi Wu, Ming Hai Yu, Yue Yang, Yong Hong Yan, Wei Fan, Ke Gong Dong, Feng Lu, Tian Kui Zhang, and Yu Qiu Gu

Laser Fusion Research Center, China Academy of Engineering Physics, Mianyang, China

Correspondence should be addressed to Fang Tan; tanfang@caep.cn

Received 26 October 2021; Revised 24 March 2022; Accepted 7 July 2022; Published 17 September 2022

Academic Editor: Yongtao Zhao

Copyright © 2022 Fang Tan et al. This is an open access article distributed under the Creative Commons Attribution License, which permits unrestricted use, distribution, and reproduction in any medium, provided the original work is properly cited.

In order to establish a compact all-optical Thomson scattering source, experimental studies were conducted on the 45 TW Ti: sapphire laser facility. By including a steel wafer, mixed gas, and plasma mirror into a double-exit jet, several mechanisms, such as shock-assisted ionization injection, ionization injection, and driving laser reflection, were integrated into one source. So, the source of complexity was remarkably reduced. Electron bunches with central energy fluctuating from 90 to 160 MeV can be produced. Plasma mirrors were used to reflect the driving laser. The scattering of the reflected laser on the electron bunches led to the generation of X-ray photons. Through comparing the X-ray spots under different experimental conditions, it is confirmed that the X-ray photons are generated by Thomson scattering. For further application, the energy spectra and source size of the Thomson scattering source were measured. The unfolded spectrum contains a large amount of low-energy photons besides a peak near 67 keV. Through importing the electron energy spectrum into the Monte Carlo simulation code, the different contributions of the photons with small and large emitting angles can be used to explain the origin of the unfolded spectrum. The maximum photon energy extended to about 500 keV. The total photon production was 10^7/pulse. The FWHM source size was about 12 μm.

1. Introduction

When photons are scattered by relativistic electrons, the so-called Thomson scattering process can increase the photon energy by approximately $4\gamma^2$ times [1, 2], where γ is the normalized electron energy. Based on this process, the Thomson scattering source possesses a set of valuable features, including compactness, tunable photon energy, potential for the duration of femtosecond time scale, and high brightness [3, 4]. In many application areas, such as phase-contrast imaging of organisms [5], shadow imaging of high-Z materials [6], stimulating nuclear resonance fluorescence (NRF) of specific isotopes [7–9], and ultra-fast pump-probe detection of transient physical and chemical processes [10], the Thomson scattering source may play a unique role.

For established, conventional Thomson scattering sources [11–15], where the electrons are produced by a classical electron accelerator, the huge size and ultra-expensive cost required by the large-scale classical electron accelerators restrict further applications. As an improvement, an all-optical Thomson scattering X-ray source has been proposed by Catravas et al. in 2001 [16], where the electrons are produced by the laser-plasma wakefield accelerator. This accelerator can produce quasi-monoenergetic electron beams with low divergence, small energy spread, and ultra-short pulse duration [17–19]. Due to the ultra-high accelerating gradient, electrons can be accelerated toward tens of MeV to several GeV within a distance of mm scale [20–23]. So, the all-optical Thomson scattering source is a very promising way to establish a compact, ultra-fast, quasi-monoenergetic X-ray source.

The first successful experimental results of all-optical Thomson scattering sources were obtained in 2006 [24], where photons with energies ranging from 400 eV to 2 keV were produced by two counter-propagating laser pulses. Based on these two laser collision models, several studies have been conducted, including the improvement of the source stability [25, 26], extending the electron maximum energy to 18 MeV through nonlinear Thomson scattering

https://doi.org/10.1155/2022/4132792 Published online by Cambridge University Press

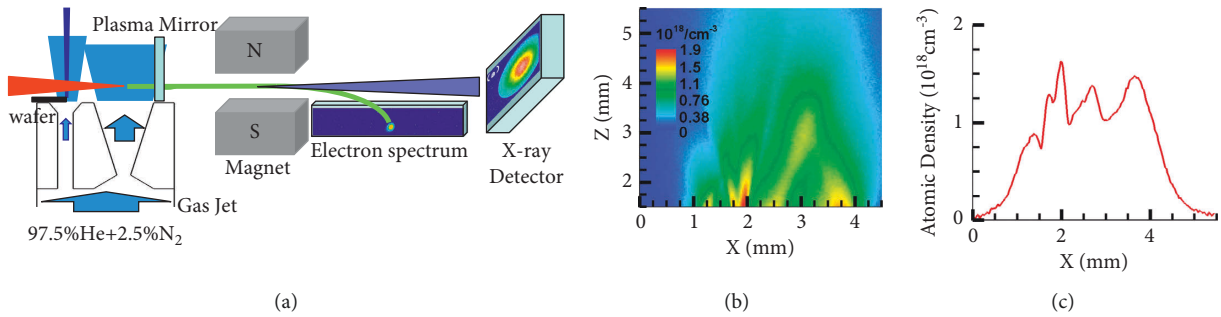


FIGURE 1: (a) The gas jet designment and the experimental layout. The view of the gas jet is enlarged. (b) The side view of the gas density distribution. (c) The one-dimensional electron density at a height of 2 mm from the gas jet.

[27], and a way to obtain sources with tunable energy [28]. High-order multiphoton (n, 500) Thomson scattering signals were also obtained in 2017 [29]. In 2012, a compact all-optical Thomson scattering source was reported [30], where a plasma mirror (PM) was used to directly reflect the driving laser. In this method, the temporal and spatial synchronization between laser and electrons can be realized more easily. Several compact all-optical Thomson scattering sources have been established based on this method [31–34].

In order to improve the stability of the generation of wakefield electrons and Thomson scattering sources, the shock assistant ionization injection technique has proved its validity [35, 36]. The studies on the cascaded acceleration technique [37–39] also show the advantages of this technique for producing high-quality electrons. The above studies show that the integration of multi-injection technologies within one accelerator has the potential to generate Thomson scattering sources with better stability and higher production. But at present, the studies on the all-optical Thomson scattering source containing multi injection and acceleration techniques are insufficient.

The integration of multitechnologies within one accelerator requires proper designing on the compactness of the accelerator. In our previous studies [40], we have established a compact laser wakefield accelerator where shock-assisted ionization injection and ionization injection were integrated into a double-exit gas jet. Based on this accelerator and a plasma mirror attached to the gas jet, a compact all-optical Thomson scattering source can be established.

In the following paragraphs, the experimental layout and the obtained electron energy spectra are shown. Then, after the driving laser was reflected by the plasma mirror, the scattering of the reflected laser on the electron bunch led to the generation of X-ray photons. Through comparing the X-ray spots under different experimental conditions, it is confirmed that the X-ray photons were produced by Thomson scattering. The location of the plasma mirror was also optimized. At last, the energy spectra and source size of the Thomson scattering source were measured for further application.

2. Experimental Parameters

The experiments were performed on the 45 TW, 25 fs, 800 nm Ti: sapphire laser facility at the Laser Fusion Research Center of CAEP in Mianyang. The laser is linearly polarized in the horizontal direction. The laser focal spot is $11.9 \times 7.8\,\mu$m full width at half maximum (FWHM) with 60% energy in the spot. In the experiments, the initial input power was set at 28 TW. The total energy coupling efficiency to the target is 70%. So, the peak laser intensity at the focus is $I = 1.81 \times 10^{19}\,\mathrm{W/cm^2}$, corresponding to a normalized intensity of $a_0 = 2.9$. The experimental layout is shown in Figure 1(a). A gas jet containing two nozzles is used as the target. The first nozzle is a cylindrical hole with an exit diameter of 1 mm and higher gas pressure. The second nozzle is a conical hole with an exit diameter of 2 mm and lower gas pressure. The shock front is produced by the impact between the gas jets from the two nozzles. The addition of a wafer can reduce the exit size of nozzle 1, leading to higher jet density and a shock front with higher density and a steeper falling edge. Mixed gas containing 97.5% He and 2.5% N_2 is used. In the first nozzle, the electron is injected from shock-assisted ionization injection. Then, the accelerated electrons are injected into the second nozzle. A 75 m thick plasma mirror (PM) made of polyethylene terephthalate (PET) is attached to the exit edge of the second nozzle. After being reflected by the plasma mirror, the driving laser interacts with the wakefield electrons for the second time, generating X-ray photons.

A spectrometer consisting of a permanent magnet (0.8 T with a length of 230 mm) and a phosphor screen imaged using a 16-bit CCD camera is used to deflect the electrons and measure the electron energy spectra. The produced X-ray photons emit out of the vacuum chamber through a 300 μm beryllium window. An X-ray camera consisting of a CsI: Tl scintillator, a fiber taper, and a 16-bit CCD sensor records the spatial distribution of the X-ray photons. The X-ray spectra are measured by using a filter stack spectrometer [41]. The X-ray source size is measured using the knife-edge imaging method [42].

3. Experimental Results

In our previous works, we established a laser wakefield accelerator with a mixed injection mechanism [40]. Based on this accelerator, stable monoenergetic wakefield electron beams with a central energy of 60 MeV were experimentally obtained. To increase the electron energy, the gas pressure of

https://doi.org/10.1155/2022/4132792 Published online by Cambridge University Press

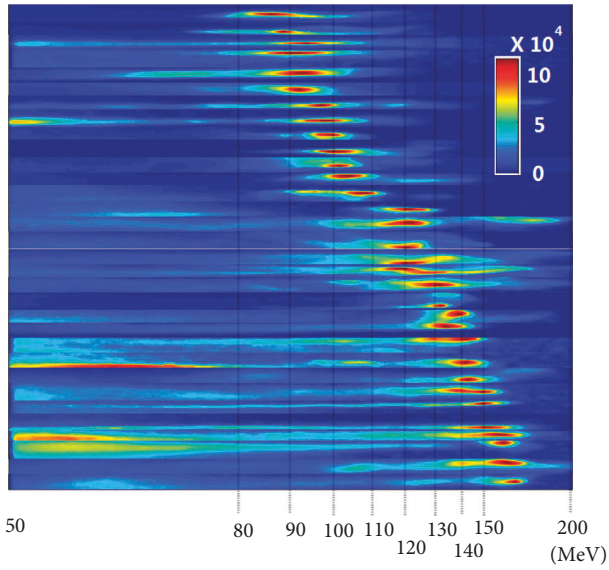


FIGURE 2: The electron energy spectra under a gas pressure of 1100 kPa.

the jet was increased from 650 kPa to 1100 kPa. Under the higher gas pressure, electrons can be steadily produced, but the electron central energy fluctuates from 90 MeV to 160 MeV, as shown in Figure 2. All of the electron energy spectra in this paper are on the same color bar as in Figure 2. The instability of electron spectra in Figure 2 comes from the instability of the gas pressure and laser energy. The nonlinear evolution of the laser in the relatively high gas pressure (1100 kPa) also leads to the fluctuation of electron energy. Actually, when the gas pressure was adjusted to about 600 kPa as in our previous experiments [40], the electron spectra with better stability and lower production were obtained. In our further studies, the optimization of the gas jet may lead to a better control of the injection process and smaller energy spread. The improvement in the stability and output power of the laser facility may lead to more stable electron production and higher electron energy.

Based on this accelerator, several kinds of X-ray sources can be produced. A Thomson scattering source can be produced through the scattering of the reflected driving laser on the electrons. Betatron radiation with photon energy ranging from hundreds of electronvolts to several tens of kiloelectron volts can be produced through the oscillation of the electrons in the wakefield. Bremsstrahlung can be produced when the electrons penetrate the plasma mirror. The direct interaction between the driving laser and the plasma mirror may also produce bremsstrahlung. To distinguish the signals of Thomson scattering from the other sources, the X-ray spots under different conditions are recorded as shown in Figure 3. In Figure 3(a), a pristine plasma mirror is used, and wakefield electrons are efficiently produced. All of the possible signals, such as signals from the Thomson scattering, Betatron radiation, and bremsstrahlung, could be produced and recorded by the X-ray camera. Figure 3(a) shows that strong and clear X-ray signals were recorded. Then, when there is no plasma mirror, the driving laser cannot be reflected. Bremsstrahlung and Thomson scattering radiation cannot be generated. Betatron radiation can be generated, but only photons with energy higher than 2 keV can penetrate the beryllium window and get recorded by an X-ray camera. The obtained result is shown in Figure 3(b), where no obvious signal is recorded. When the plasma mirror was placed farther from the gas jet, defocusing of the laser reduced the corresponding intensity. So, the laser reflection on the plasma mirror and the radiation intensity from the Thomson scattering were drastically reduced. Only Betatron radiation and bremsstrahlung can be produced as a result of electron-plasma mirror interaction. But similar to Figure 3(b), the recorded result in Figure 3(c) shows no obvious result. So, it is clear that the contributions of betatron radiation and bremsstrahlung can be ignored.

Finally, the variability of the electron injection at higher pressures causes instability of the wakefield acceleration. Some shots under the same conditions as in Figure 3(a) resulted in poor electron beam generation. Figure 3(d) gives an example of such a result with no obvious X-ray images from Thomson scattering. All of the results in Figure 3 show that only with pristine, properly placed plasma mirror, and efficient laser wakefield acceleration, distinct X-ray signals can be recorded. Only effective Thomson scattering can result in the X-ray spot as shown in Figure 3(a). In Figure 3(a), the FWHM emitting angle of the X-ray source is 30 mrad.

To find the optimized position of the plasma mirrors, the average intensity of the X-ray spots recorded by CCD at different plasma mirror positions is shown in Figure 4. In this figure, position 0 corresponds to the exit edge of the gas jet. When the plasma mirror moves away from the gas jet, it moves from the edge part of the gas jet to a vacuum. The optimized plasma mirror position of 0.1 mm shown in Figure 4 reflects the position in the edge part of the gas jet with the highest laser reflectivity. Then, in vacuum, when the plasma mirror moves away from the gas jet, the laser beam size increases at the colliding point, leading to a decrease in laser intensity, reflectivity, and X-ray intensity. The incidence angle of laser photons in vacuum may be larger than the incidence angle of the guided laser in the gas jet. So qualitatively, the energy spread of the X-ray spectra in vacuum will be larger than that in the gas jet. But when the plasma mirror moves in vacuum, the interaction angles between electrons and laser photons stay unchanged, leading to a nearly unchanged spectra profile.

Next, we used the previously established filter stack spectrometer [41] to measure the energy spectra of the obtained Thomson scattering source. For the electron bunch with the energy spectrum as in Figure 5(a), the different X-ray profiles behind a set of stacked filters are shown in Figure 5(b). Based on the results in Figure 5(b), the input X-ray spectrum within the emitting angle of 20 mrad can be unfolded. The unfolded spectrum in Figure 5(c) shows that the spectrum contains a large number of low-energy photons besides a peak near 67 keV. The maximum photon energy extends to about 500 keV. In the electron energy spectrum in Figure 5(a), there is a small part of electrons with energy of 150 MeV. So, the production of photons with energy of

https://doi.org/10.1155/2022/4132792 Published online by Cambridge University Press

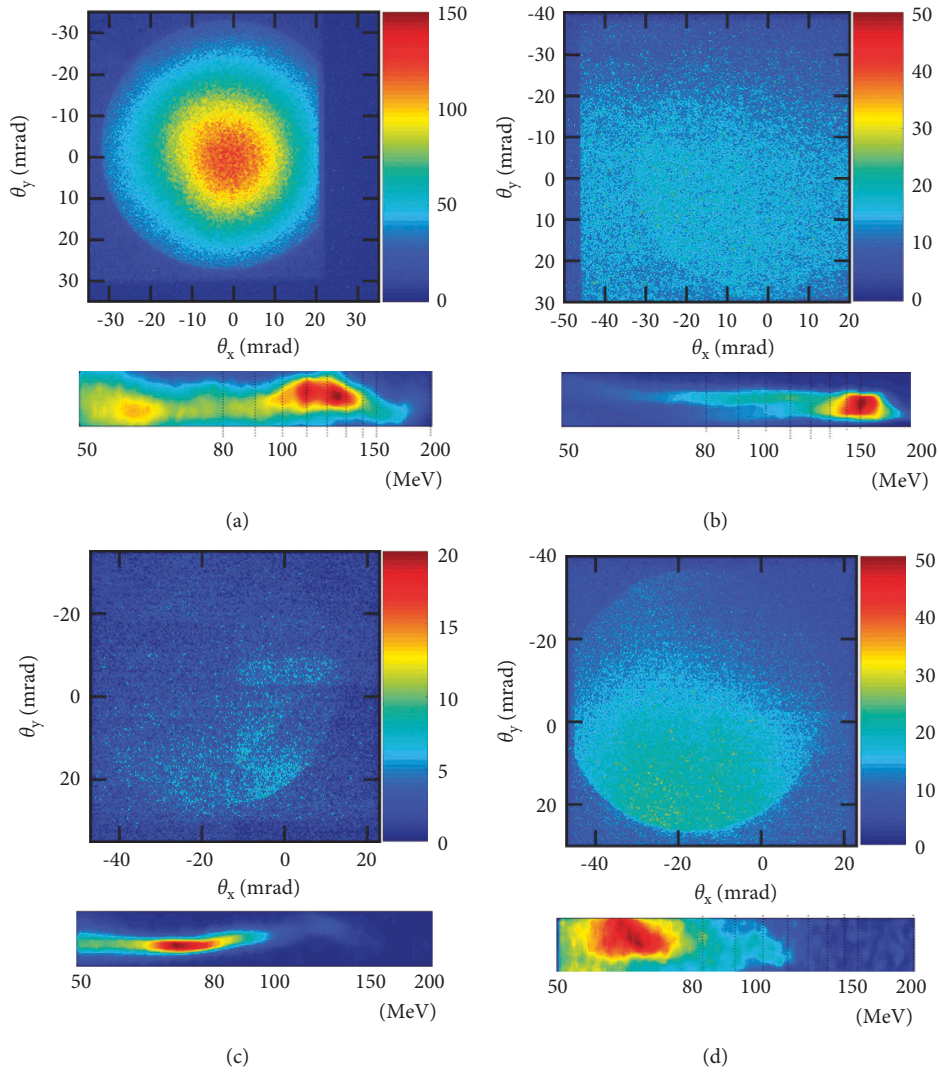


FIGURE 3: The X-ray spots under different experimental conditions and the corresponding electron spectra.

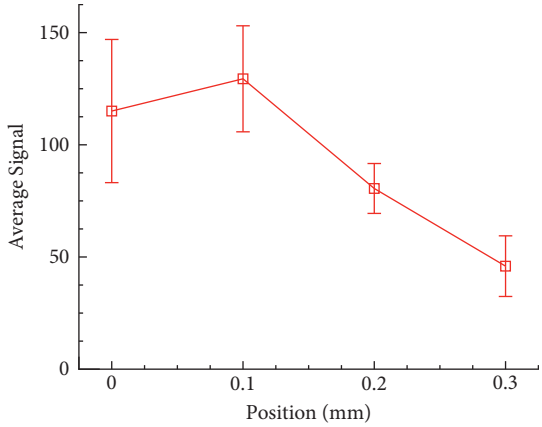


FIGURE 4: The average intensity of X-ray spots versus the plasma mirror position.

500 keV can be attributed to the Thomson scattering of laser photons on these high-energy electrons. The contribution of the nonlinear Thomson scattering effect should also be considered. In our experiments, the peak laser intensity at the focus is $I = 1.81 \times 10^{19}$ W/cm, corresponding to a normalized intensity of $a_0 = 2.9$. The laser spot at 0.1 mm away from the jet exit is nearly unchanged. If the reflectivity on the plasma mirror is assumed to be 50%, the intensity of the reflected can be estimated as 0.9×10^{19} W/cm, corresponding to normalized intensity $a_0 = 2.05$. So, under this intensity, the nonlinear Compton scattering effect may lead to an inapparent contribution. Based on the obtained spectrum in Figure 5(c), the total photon production can be estimated as 10^7/pulse.

In order to find the origin of these low-energy photons, the electron energy spectrum in Figure 5(a) can be imported into the Monte Carlo simulation code CAIN [43] to obtain the theoretical radiation spectrum. The calculation parameters are the same as the experimental parameters. The relation between photon energy and emitting angle is shown in Figure 6(a), which is a traditional angular-energy distribution of the Thomson scattering source. The red and yellow dots in Figure 6(a) correspond to the microphotons

https://doi.org/10.1155/2022/4132792 Published online by Cambridge University Press

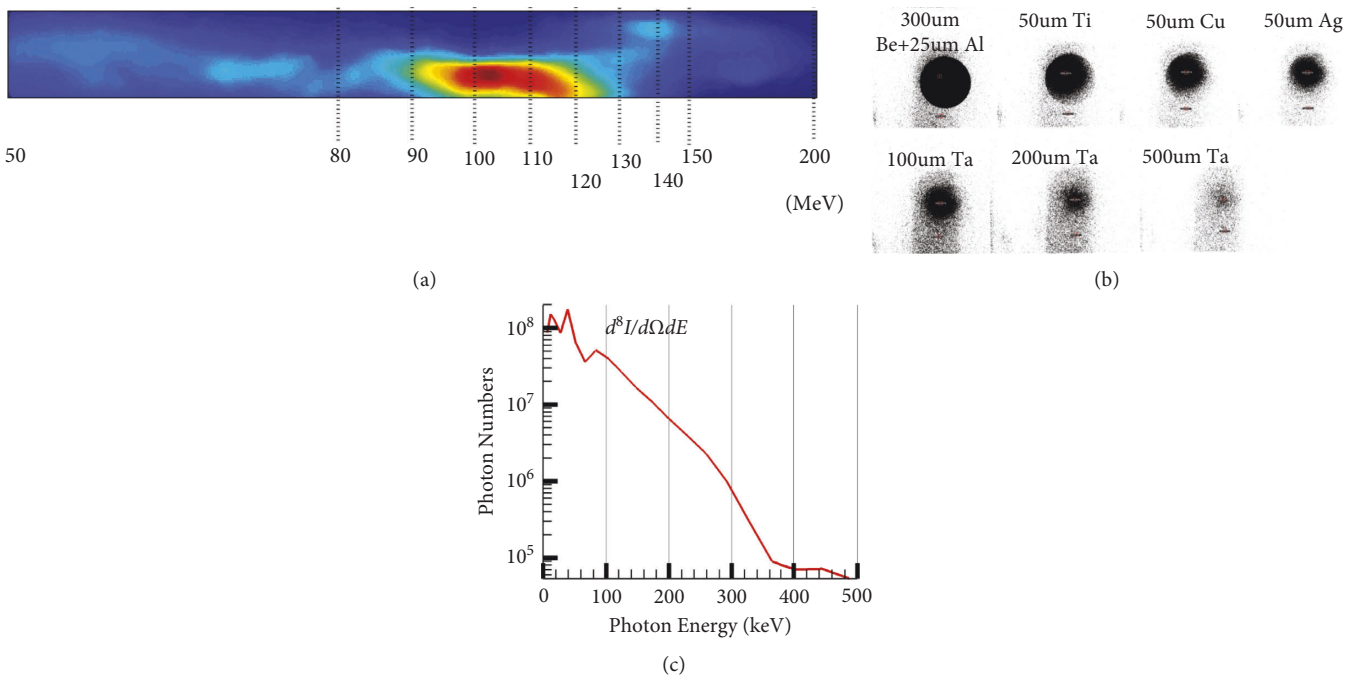


FIGURE 5: (a) The electron energy spectrum. (b) The corresponding X-ray profiles behind a set of stacked filters. (c) The unfolded spectrum.

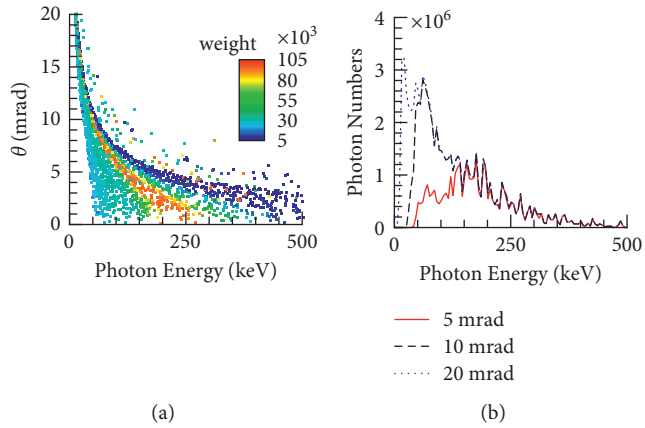


FIGURE 6: (a) The relation between photon energy and emitting angle. Weight is the photon number of each microparticle. (b) The integrated energy spectra of the emitting photons for an integration angle of 5, 10, and 20 mrad.

with the highest weight, reflecting the electrons in the peak of the electron energy spectrum in Figure 5(a). Due to momentum and energy conservation, the energy of the photons scattered toward a larger angle is always smaller. On the contrary, photons with higher energy mainly emit out within an angle smaller than 5 mrad. The integrated photon energy spectra for integration angles of 5, 10, and 20 mrad are shown in Figure 6(b). The red solid line in Figure 6(b) shows that the photons emitting out at an angle of 5 mrad mainly contribute to the higher energy part of the spectrum. When photons within a larger emitting angle are included in the integration, the black and blue dashed lines in Figure 6(b) show that the low-energy part of the spectra is drastically enhanced. The different contributions of the photons with small and large emitting angles can be used to explain the similar spectral shapes in Figures 5(c) and 6(b). But restricted by the limited filter numbers in the filter stack spectrometer, the photon energy of the unfold spectrum in Figure 5(c) is a bit lower than the calculated results in Figure 6(b). In our further studies, the energy spectra may be more precisely measured with the improvement in the filter stack spectrometer.

The obtained source can be used for radiography, where the resolution is one of the most important parameters. For a knife-edge made of 100 μm lead foil, its radiograph image is shown in Figure 7(a). If the source profile is set as a Gaussian shape, the unfolded source size (FWHM) is 12 μm, as shown in Figure 7(b). It also shows that a gold grid used in the electron microscope with a grid size of 2000 mesh × 12.5 μm pitch per inch and a diameter of 3.05 mm was also used. The thickness of

https://doi.org/10.1155/2022/4132792 Published online by Cambridge University Press

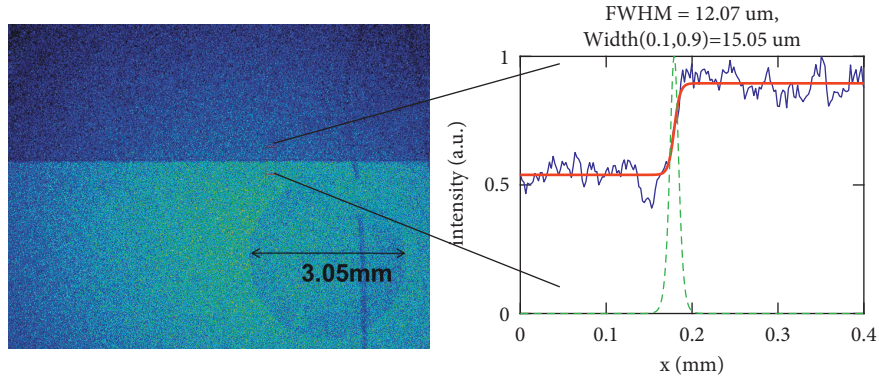


Figure 7: (a) Radiograph of a knife-edge and a gold grid. (b) The unfolded source size.

the grid is only 3 μm, so the radiation source directly penetrates the grid, leading to a fuzzy circle in Figure 7.

4. Summary and Discussion

This work reports our studies on the compact all-optical Thomson scattering source. By including a steel wafer, mixed gas, and plasma mirror into a double-exit jet, several mechanisms, such as shock-assisted ionization injection, ionization injection, and driving laser reflection, are integrated. In this compact source, only one gas supply system is required. The source complexity is remarkably reduced. The laser wakefield accelerator with a mixed injection mechanism can steadily produce electron bunches with a central energy fluctuating from 90 MeV to 160 MeV. Then, the driving laser is reflected by the plasma mirror and scatters on the electron bunch, leading to the generation of X-ray photons. By comparing the X-ray spots under different experimental conditions, it is confirmed that the recorded signals by the X-ray camera are produced by Thomson scattering. For further application, we used a filter stack spectrometer to measure the X-ray energy spectra. The unfolded spectrum has a similar spectral shape to the calculated results, which can be explained by different contributions of photons at small and large emitting angles. The maximum photon energy extends to about 500 keV. The total photon production is 10^7/shot. By using the knife-edge method, the FWHM source size can be measured as about 12 μm.

In our further studies, the optimization of the gas jet may lead to better control of the injection process and smaller energy spread. The improvement in the stability and output power of the laser facility may lead to a more stable electron production and higher electron energy. Moreover, the energy spectra and source size can be more precisely measured with the modification of the corresponding diagnostic techniques.

Data Availability

The data, models, and code generated or used in this study are included within the article.

Conflicts of Interest

The authors declare that they have no conflicts of interest.

Acknowledgments

This work was supported by the Science Challenge Program (TZ2018005), the Presidential Foundation of China Academy of Engineering Physics (2014-1-017), NSAF (U1630246), and the National Key R & D Program (2016YFA0401100).

References

[1] A. Einstein, "Euclidean model of space and time," *Annals of Physics*, vol. 322, no. 10, pp. 891–921, 1905.

[2] J. J. Thomson, *Conduction of Electricity through Gases*, Cambridge University Press, Cambridge, UK, 1906.

[3] P. Sprangle, A. Ting, E. Esarey, and A. Fisher, "Tunable, short pulse hard x-rays from a compact laser synchrotron source," *Journal of Applied Physics*, vol. 72, no. 11, pp. 5032–5038, 1992.

[4] P. Sprangle and E. Esarey, "Interaction of ultrahigh laser fields with beams and plasmas," *Physics of Fluids B: Plasma Physics*, vol. 4, no. 7, pp. 2241–2248, 1992.

[5] D. Attwood, *Soft X-Rays and Extreme Ultraviolet Radiation: Principles and Applications*, Cambridge University Press, Cambridge, UK, 1999.

[6] C. J. Joshi and P. B. Corkum, "Interactions of ultra-intense laser light with matter," *Physics Today*, vol. 48, no. 1, pp. 36–43, 1995.

[7] F. Albert, "Compton scattering source and applications at LLNL," *AIP Conference Proceedings*, vol. 1299, p. 550, 1995.

[8] K. Ali, H. Zen, H. Ohgaki et al., "Fusion visualization technique to improve a three-dimensional isotope-selective CT image based on nuclear resonance fluorescence with a gamma-CT image," *Applied Sciences*, vol. 11, no. 24, Article ID 11866, 2021.

[9] H. Y. Lan, T. Song, Z. H. Luo, J. L. Zhou, Z. H. Zhu, and W. Luo, "Isotope-sensitive imaging of special nuclear materials using computer tomography based on scattering nuclear resonance fluorescence," *Physical Review Applied*, vol. 16, no. 5, Article ID 054048, 2021.

https://doi.org/10.1155/2022/4132792 Published online by Cambridge University Press

[10] R. A. Wilhelm, E. Gruber, J. Schwestka et al., "Interatomic coulombic decay: the mechanism for rapid deexcitation of hollow atoms," *Physical Review Letters*, vol. 119, no. 10, Article ID 103401, 2017.

[11] D. J. Gibson, S. G. Anderson, C. P. J. Barty et al., "PLEIADES: a picosecond compton scattering X-ray source for advanced backlighting and Time-resolved material studies," *Physics of Plasmas*, vol. 11, no. 5, pp. 2857–2864, 2004.

[12] W. P. Leemans, R. W. Schoenlein, P. Volfbeyn et al., "X-ray based subpicosecond electron bunch characterization using 90 Thomson scattering," *Physical Review Letters*, vol. 77, no. 20, pp. 4182–4185, 1996.

[13] I. V. Pogorelsky, I. Ben-Zvi, T. Hirose et al., "Demonstration of 8×1018 photons/second peaked at 1.8 Å in a relativistic Thomson scattering experiment," *Physical Review ST Accelerators Beams*, vol. 3, no. 9, Article ID 090702, 2000.

[14] R. W. Schoenlein, W. P. Leemans, A. H. Chin et al., "Femtosecond X-ray pulses at 0.4 Å generated by 90° Thomson scattering: a tool for probing the structural dynamics of materials," *Science*, vol. 274, no. 5285, pp. 236–238, 1996.

[15] C. X. Huang, W. H. Pan, R. K. Li et al., "Tsinghua Thomson scattering X-ray source," *Nuclear Instruments and Methods A*, vol. 608, no. 1, pp. S70–S74, 2009.

[16] P. Catravas, E. Esarey, and W. P. Leemans, "Femtosecond X-rays from Thomson scattering using laser wakefield accelerators," *Measurement Science and Technology*, vol. 12, no. 11, pp. 1828–1834, 2001.

[17] E. Esarey, R. F. Hubbard, W. P. Leemans, A. Ting, and P. Sprangle, "Electron injection into plasma wakefields by colliding laser pulses," *Physical Review Letters*, vol. 79, no. 14, pp. 2682–2685, 1997.

[18] E. Esarey, C. B. Schroeder, W. P. Leemans, and B. Hafizi, "Laser induced electron trapping in plasma-based accelerators," *Physics of Plasmas*, vol. 6, no. 5, pp. 2262–2268, 1999.

[19] D. Umstadter, J. K. Kim, and E. Dodd, "Laser injection of ultrashort electron pulses into wakefield plasma waves," *Physical Review Letters*, vol. 76, no. 12, pp. 2073–2076, 1996.

[20] J. Faure, Y. Glinec, A. Pukhov et al., "A laser-plasma accelerator producing monoenergetic electron beams," *Nature*, vol. 431, no. 7008, pp. 541–544, 2004.

[21] C. G. R. Geddes, C. Toth, J. van Tilborg et al., "High-quality electron beams from a laser wakefield accelerator using plasma-channel guiding," *Nature*, vol. 431, no. 7008, pp. 538–541, 2004.

[22] A. J. Gonsalves, K. Nakamura, J. Daniels et al., "Petawatt laser guiding and electron beam acceleration to 8 GeV in a laser-heated capillary discharge waveguide," *Physical Review Letters*, vol. 122, Article ID 084801, 2019.

[23] S. P. D. Mangles, C. D. Murphy, Z. Najmudin et al., "Monoenergetic beams of relativistic electrons from intense laser-plasma interactions," *Nature*, vol. 431, no. 7008, pp. 535–538, 2004.

[24] H. Schwoerer, B. Liesfeld, H.-P. Schlenvoigt, K.-U. Amthor, and R. Sauerbrey, "Thomson-backscattered X rays from laser-accelerated electrons," *Physical Review Letters*, vol. 96, no. 1, Article ID 014802, 2006.

[25] S. Chen, N. D. Powers, I. Ghebregziabher et al., "MeV-energy X rays from inverse compton scattering with laser-wakefield accelerated electrons," *Physical Review Letters*, vol. 110, no. 15, Article ID 155003, 2013.

[26] N. D. Powers, I. Ghebregziabher, G. Golovin et al., "Quasi-monoenergetic and tunable X-rays from a laser-driven Compton light source," *Nature Photonics*, vol. 8, no. 1, pp. 28–31, 2013.

[27] G. Sarri, D. J. Corvan, W. Schumaker et al., "Ultrahigh brilliance multi-MeVγ-ray beams from nonlinear relativistic Thomson scattering," *Physical Review Letters*, vol. 113, no. 22, Article ID 224801, 2014.

[28] K. Khrennikov, J. Wenz, A. Buck et al., "Tunable all-optical quasimonochromatic Thomson X-ray source in the nonlinear regime," *Physical Review Letters*, vol. 114, no. 19, Article ID 195003, 2015.

[29] W. C. Yan, C. Fruhling, G. Golovin et al., "High-order multiphoton Thomson scattering," *Nature Photonics*, vol. 11, no. 8, pp. 514–520, 2017.

[30] K. Ta Phuoc, S. Corde, C. Thaury et al., "All-optical compton gamma-ray source," *Nature Photonics*, vol. 6, no. 5, pp. 308–311, 2012.

[31] Y. Ma, J. F. Hua, D. X. Liu et al., "Region-of-interest microfocus computed tomography based on an all-optical inverse compton scattering source," *Matter and Radiation at Extremes*, vol. 5, no. 6, Article ID 064401, 2020.

[32] H. E. Tsai, X. M. Wang, J. M. Shaw et al., "Compact tunable compton x-ray source from laser-plasma accelerator and plasma mirror," *Physics of Plasmas*, vol. 22, no. 2, Article ID 023106, 2015.

[33] C. H. Yu, R. Qi, W. T. Wang et al., "Ultrahigh brilliance quasi-monochromatic MeV -rays based on self-synchronized all-optical compton scattering," *Scientific Reports*, vol. 6, no. 1, Article ID 29518, 2016.

[34] C. Q. Zhu, J. G. Wang, J. Feng et al., "Inverse compton scattering x-ray source from laser electron accelerator in pure nitrogen with 15 TW laser pulses," *Plasma Physics and Controlled Fusion*, vol. 61, no. 2, Article ID 024001, 2018.

[35] A. Buck, J. Wenz, J. Xu et al., "Shock-front injector for high-quality laser-plasma acceleration," *Physical Review Letters*, vol. 110, no. 18, Article ID 185006, 2013.

[36] C. Thaury, E. Guillaume, A. Lifschitz et al., "Shock assisted ionization injection in laser-plasma accelerators," *Scientific Reports*, vol. 5, no. 1, Article ID 16310, 2015.

[37] G. Golovin, S. Chen, N. Powers et al., "Tunable monoenergetic electron beams from independently controllable laser-wakefield acceleration and injection," *Physical Review ST Accelerators and Beams*, vol. 18, no. 1, Article ID 011301, 2015.

[38] J. S. Liu, C. Q. Xia, W. T. Wang et al., "All-Optical cascaded laser wakefield accelerator using ionization-induced injection," *Physical Review Letters*, vol. 107, no. 3, Article ID 035001, 2011.

[39] W. T. Wang, W. T. Li, J. S. Liu et al., "High-brightness high-energy electron beams from a laser wakefield accelerator via energy chirp control," *Physical Review Letters*, vol. 117, no. 12, Article ID 124801, 2016.

[40] F. Tan, X. H. Zhang, B. Zhu et al., "Mixed injection mechanism assisted cascaded laser wakefield accelerator," *Acta Physica Sinica*, vol. 68, no. 17, Article ID 175201, 2019.

[41] M. H. Yu, T. Tan, Y. H. Yan et al., "A filter stack spectrometer for spectrum measurement of laser generated gamma ray, developlasma mirrorent of filter stack spectrometer for spectrum measurement of X ray generated by laser," *Atomic Energy Science and Technology*, vol. 51, p. 1090, 2017.

[42] S. Kneip, C. McGuffey, J. L. Martins et al., "Bright spatially coherent synchrotron X-rays from a table-top source," *Nature Physics*, vol. 7, no. 9, p. 737, 2011.

[43] P. Chen, G. A. Hortonsmith, T. Ohgaki, A. W. Weidemann, and K. Yokoya, "CAIN: conglomrat d'ABEL et d'interactions non-linaires," *Nuclear Instruments and Methods A*, vol. 355, p. 107, 1994.

https://doi.org/10.1155/2022/4132792 Published online by Cambridge University Press